Pergamon

Acta mater. 49 (2001) 4337–4346

Acta MATERIALIA

www.elsevier.com/locate/actamat

COMBINED MODEL OF DISLOCATION MOTION WITH THERMALLY ACTIVATED AND DRAG-DEPENDENT STAGES

M. HIRATANI‡ and E. M. NADGORNY†

Department of Physics, Michigan Technological University, Houghton, MI 49931, USA

(Received 29 March 2001; received in revised form 6 July 2001; accepted 6 July 2001)

Abstract—A computational model is developed to study the effect of coupling of thermally activated and drag-dependent processes during dislocation motion through an array of obstacles in metals. The model explicitly includes three successive, reiterative stages typical of such motion: the thermally activated break-off from an equilibrium position; accelerated drag-dependent motion; and the transition to the next equilibrium position controlled by the two previous stages. Calculation results are presented over a wide range of dislocation velocities, applied stresses and temperatures for a prototype f.c.c. metal close to copper. The presented model is also the first step for explaining quantitatively experimental findings regarding the effects of the SN transition on dislocation motion and plasticity in superconductors.

Keywords: Metals; Dislocations (mobility and theory); Thermally activated processes; Dynamic phenomena

1. INTRODUCTION

Dislocations define plastic deformation and its features in all crystalline materials. In computer simulations of dislocation behavior, the relationship between the velocity of individual dislocations and the applied stress is of increasing interest. Many *in situ* straining electron microscopic studies have shown that the dislocation glide in many materials is intrinsically jerky and consists of successive fast runs of dislocation segments from one local obstacle to the next, as evidenced in Messerschmidt [1]. Numerous experimental measurements of the average dislocation velocity v as a function of the applied stress σ and temperature T have also demonstrated that there are two different regions in the dependence $v(\sigma,T)$, with quite different dislocation behavior. In one region (roughly between 10^{-6} and 1 m/s), $v(\sigma)$ is non-linear, and obstacles have a strong effect on the velocity v. In the other region (above about 1 m/s), $v(\sigma)$ is linear and only weakly depends on obstacles. The temperature dependence of the velocity in the first, lower-velocity region obeys Arrhenius-type law, i.e. the velocity increases with temperature; in the second region the temperature dependence is reversed.

There is a general consensus on the predominant mechanisms responsible for these velocity features. In the first region, the dislocation motion is thermally activated, and local obstacles of various types and the Peierls lattice barrier control the glide resistance; in the second, the motion is drag-dependent, and phonons and electrons are responsible for the drag resistance. Two-dimensional computer simulations, computational studies, and analytical calculations have made major contributions to the current understanding of many details of these mechanisms, as documented in Kaganov *et al.* [2] Kocks *et al.* [3], Nadgorny [4], Alshits [5], and Indenbom and Chernov [6]. Traditionally, however, these two regions are considered separately, and only in several studies attempts have been made to combine them. The first calculations of the dislocation velocity that explicitly included both a dislocation drag and point obstacles were performed by Frost and Ashby [7]. However, they considered only regular obstacles arrays and neglected both obstacle randomness and dislocation inertia. Suenaga and Galligan [8], Granato [9], and Komada and Yoshiyama [10] proposed independently a phenomenological dislocation inertial model for an enhanced plasticity in superconductors. The model suggests that a moving dislocation can overcome obstacles by inertial overshooting if the dislocation velocity is high enough. Such a situation can occur when dislocation segments undergo a transition from the damped to underdamped state due to a change in the dislocation drag. Although the inertial model

† To whom all correspondence should be addressed. Tel.: +1-906-487-2393; fax: +1-906-487-2933.

E-mail address: nadgorny@mtu.edu (E. M. Nadgorny)

‡ Present address: School of Mechanical and Materials Engineering, Washington State University, Pullman, WA 99164, USA.

1359-6454/01/$20.00
PII: S1359-6454(01)00266-X

seems to be promising, Estrin [11] showed that any considerable effect of inertia, as suggested by the model, could be realized only in the vicinity of the critical (athermal) stress. Schwartz and Labusch [11, 12] were the first to combine the thermally activated and drag-dependent mechanisms more adequately but their model could be applied only to rather high velocities, again near or above the critical stress. Landau [14] suggested a more consistent approach: he considered both of the two main mechanisms together at the low-velocity regime and showed how to implement the inertial effect through a number of obstacles overcome athermally; however, he made several mistakes in the calculations. Isaac and Granato [15] criticized the Landau model as not based on physical principles. They proposed their own model exploiting the equations of Brownian motion and applying them to dislocation motion. However, since they developed essentially a one-dimensional model, they were unable to take into consideration obstacle randomness and other features of the two-dimensional dislocation motion.

As a first step in comprehensive computing the dislocation velocity in metals over a wide range of stresses and temperature, a general model of dislocation motion is developed. This paper discusses the physical arguments for the model based on computer simulation results and an extension of the Schwartz–Labusch and Landau models. We consider the dislocation motion in two dimensions through an array of N random obstacles and show how to include explicitly the dynamic inertial breakaway of underdamped dislocation segments in the model. We briefly review the existing theories of the dislocation drag coefficient and estimate its main phonon and electron contributions, including effect of the Peierls barrier, to establish possible ranges of the dynamic effect. Next, we use a model material (with a copper as a prototype) to calculate the stress, temperature and obstacle density dependences of the dislocation velocity. Finally, we show that the model is in good agreement with experiments on dislocation mobility, yield stress and the strain rate sensitivity.

2. MODEL DESCRIPTION

2.1. Model basic concepts

Several assumptions are made in the present study, all of them being in agreement with numerous computer simulations of thermally activated dislocation motion. The dislocation of the Burgers vector b is considered as a flexible string able to bow out in a glide plane between N identical discreet obstacles randomly distributed with the average spacing L. The dislocation has a constant line tension $\Gamma = \mu b^2/2$, where μ is the shear modulus. The applied shear stress σ causes each dislocation segment to bow out to an equilibrium radius of curvature, $R = \Gamma/b\sigma$. The stress σ is reckoned from the Peierls stress τ_p, which is assumed to be $\tau_p = 2\times10^{-5}\,\mu$. When far from the obstacles, the dislocation glides against a drag resistance represented by the temperature-dependent dislocation drag coefficient B. No relativistic effect is included in high-velocity dislocation motion [16]. When closer to the obstacles, the dislocation is opposed by an obstacle resistance represented by the obstacle–dislocation interaction energy. (An example demonstrating how to include the obstacle resistance into conventional calculation of the dislocation velocity is presented in Appendix A.) The critical angle of attack 0_c represents the obstacle strength, so that the force F exerted on any obstacle by the dislocation at an equilibrium stable position is less than the critical force, $F \le F_c = 2\Gamma \sin(\theta_c/2)$ [17]. The obstacles are considered weak, $0 < \theta_c \le \pi/10$, so that the interaction between the arms of the dislocation at an obstacle can be neglected and the quasi-straight line approximation [18, 19] is satisfied. The dislocation is moving (with no climb) in the y-direction and oriented along the x-direction on average. After "waiting" in its stable position, the dislocation is released by thermal activation from the obstacle with the shortest waiting time t_w [20–22]. Then the dislocation glides to the next stable position for a running time t_{run} crossing running distance λ. If, however, the dislocation impact velocity at moment when the dislocation touches the encountered obstacles is high enough to satisfy an underdamped condition, dynamic breakaway takes place without thermal activation. In perfect analogy to the thermally activation models [14, 20], the total dislocation velocity becomes

$$v_{total} = \lambda/(t_w + t_{run}) \tag{1}$$

where the average running distance λ, the average waiting time t_w and the average running time t_{run} should be calculated to find the total dislocation velocity.

2.2. The activation free enthalpy and waiting time

Any modeling of thermally activated motion of dislocation among random obstacles requires detailed knowledge of the dislocation–obstacle interaction to calculate the activation free enthalpy ΔG. In Appendix A an example of such calculation is presented in the case of an edge straight dislocation moves in the stress field of a dilatation center when an analytical solution is possible. Since ΔG can be obtained analytically only in limited cases, an empirical expression [3, 4] is usually used,

$$\Delta G*(F*) = \Delta G/G_0 = [1-(F/F_c)^p]^q = (1-F*^p)^q \tag{2}$$

where G_0 is the total free enthalpy, and the phenomenological parameters p and q describe the obstacle

force profile, $0<p\leq 1$ and $1\leq q\leq 2$ [3], cf. Appendix A. Such an expression is extensively applied in computer simulations of dislocation motion with various sets of the phenomenological parameters, and some examples are shown in Fig. 1. As can be seen, all of the curves are relatively close, except the linear dependence (a) representing box-shaped obstacles. The free enthalpy $\Delta G^*(F^*)$ derived in Appendix A (curve d) is in the middle. Computer simulations show that the different dependences $\Delta G^*(F^*)$ not only result in a qualitatively similar dependence $v(\sigma,T)$ but also reveal the same typical features of dislocation motion [23].

In order to calculate the average waiting time t_w consistent with equation (2), scaling relations obtained from either the Friedel steady-state propagation model or computer simulation results can be used [3]. From generalized Friedel relations [4], the average dislocation segment length l and the critical stress σ_c, (which corresponds to F_c [17]) are

$$l = \alpha L(\sigma/\tau_0)^{-1/3} \tag{3}$$

$$\sigma_c = \alpha_F \tau_0 \sin^{3/2}(\theta_c/2) \tag{4}$$

where $\tau_0 = 2\Gamma/bL$ is the Orowan stress, and the coefficients α and α_F are of the order of one. Since the dislocation exerts the average force $F = b\sigma l$ on the obstacles, combining equations (3) and (4) yields the scaling law for the reduced force F^* and the reduced applied stress $\sigma* = \sigma/\sigma_c$ in a form of

$$F* = \alpha(\alpha_F \sigma*)^{2/3} \tag{5a}$$

In his original model, Friedel [24] suggested that $\alpha = \alpha_F = 1$; more sophisticated analytical calculations [18, 19, 25] showed later that α might be between 0.564 and 0.734, and α_F between 0.95 and 1.082, depending on chosen assumptions. Computer simulation [20] gives almost the same scaling law,

$$F* = (\gamma_{eff}\sigma*)^{2/3} \tag{5b}$$

where the statistical coefficient $\gamma_{eff}\approx 1.05$ reflects the fact that the activation events occur not always at the "average" segment; additionally, γ_{eff} is the same regardless of the choice of $\Delta G^*(F^*)$ in equation (2) [20, 21, 23]. Equations (5a) and (5b) can be combined to give

$$F* = (\eta\sigma*)^{2/3} \tag{5c}$$

where factor η represents either α and α_F or γ_{eff}. Equation (5c) converts the free enthalpy $\Delta G^*(F^*)$ of equation (2) into the effective free enthalpy $\Delta G*_{eff}(\sigma*)$ yielding

$$\Delta G*_{eff}(\sigma*) = \Delta G_{eff}(\sigma^*)/G_0 = [1-(\eta\sigma^*)^{2p/3}]^q \tag{6}$$

and, correspondingly for the average waiting tune t_w,

$$t_w^{-1} = \nu_d \exp(-\Delta G_{eff}/kT) = \nu_d \exp(-\Delta G^*_{eff}/T^*) \tag{7}$$

where ν_d is the dislocation attempt frequency, $T^* = kT/G_0$ the reduced temperature, k Boltzmann's constant. Obviously, any obstacle profile can be incorporated in equation (7) using the scaling law.

2.3. The running distance, the running time and dynamic inertial effect

To calculate the average running distance λ and the running time t_{run} with explicit dislocation inertia, we first consider their static quantities. The running distance λ can be obtained from the average area $\bar{a}$ swept out by the dislocation between the successive activation events. Since $\bar{a} = \lambda l$, as consistent with the Friedel model and computer simulations, we need to know first the swept area dependence $\bar{a}(\sigma,T)$. The first simulations of thermally activated dislocation motion [20, 21, 26] reveal that the swept area depends strongly on the applied stress σ and only slightly, if any, on temperature. The average swept area $\bar{a}$ equals L^2 at low stresses, which means that on average each obstacle in the array has to be overcome through thermal activation, and the athermal breakaway is negligible. As stresses increases above about $0.3\sigma_c$, more and more obstacles satisfy the breakaway criterion $\theta\geq\theta_c$, and $\bar{a}$ increases dramatically. Finally, at $\sigma = \sigma_c$ the dislocation is able to move through the entire array after the first activation, so that $\bar{a} = NL^2$. An additional point to emphasize is that the dislo-

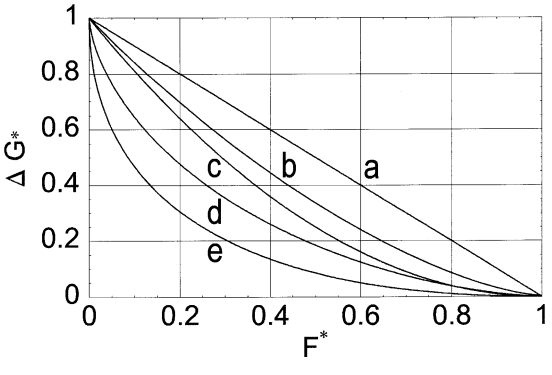

Fig. 1. Dependence of ΔG^* on F^*, equation (2) for $p = q = 1$ (curve a); $p = 1$ and $q = 2$ (c); $p = 0.63$ and $q = 1.63$ (d, according to Appendix A); $p = 1/2$ and $q = 2$ (e); Schwarz–Labusch potential [12] (b).

cation velocity was found to be practically the same if calculated either from the total swept area and the total glide time or from the average area $\bar{a}$ per activation event and the average "expectation" time t_w given in equation (7) [20, 21] Therefore, the stress-dependent running distance $\lambda(\sigma)$ can be obtained as $\lambda = \bar{a}/l$ from $\bar{a}(\sigma)$. It is convenient to express $\lambda(\sigma)$ not through $\bar{a}$ but through the increase δa of the swept area relative to the average area per obstacle, L^2, as

$$\delta a = \Delta\bar{a}/\bar{a} = (\bar{a}-L^2)/\bar{a}. \tag{8}$$

In this case, $\delta a(\sigma)$ is within the range between 0 and 1. Since the stress dependences of neither $\bar{a}$ nor δa have been derived analytically so far, we use the available computer simulation data [14, 20, 21] to obtain $\delta a(\sigma^*)$ in an empirical form through fitted parameters as†

$$\delta a = \exp\{-p_1[1-\sigma^*]^{p_2}(\sigma^*)^{-p_3}\} \tag{9}$$

where $p_1 = 1.73$, $p_2 = 1.93$, and $p_3 = 1.19$. Then from equations (8) and (9), λ becomes

$$\lambda = L^2/(1-\delta a)l \tag{10}$$

To find the running time t_{run}, we use the equation of motion of a unit dislocation length,

$$mv(\mathrm{d}v/\mathrm{d}y) + Bv - b\sigma = 0 \tag{11}$$

where y is the direction normal to the dislocation moving with the velocity $v = \mathrm{d}y/\mathrm{d}x$, m the dislocation effective mass, $m \approx \rho b^2/2$‡, and B the dislocation drag coefficient. The dislocation curvature can be neglected in equation (11) assuming $R \gg 1$. Then

$$t_{run} = -\tau_r \ln[1-(v_i/v_{visc})] \tag{12}$$

where $v_{visc} = b\sigma/B$ is the viscous velocity, $\tau_r = m/B$ the relaxation time, and v_i the dislocation impact velocity at the static equilibrium position. Notice that the average running velocity $v_{run} = \lambda/t_{run}$ is not equal to the viscous velocity in the general case, contrary to assumptions made by Landau [14, 27].

Equation (11) also allows connecting the impact velocity v_i with the running distance λ, since

$$\lambda = \int_0^{\lambda} \mathrm{d}y = \int_o^{v_i} \frac{v\tau_r}{v_{visc}-v}\,\mathrm{d}v \tag{13}$$

so that solving equation (13) in a form of

$$\lambda(v_i) = \tau_r v_{visc} \sum_{j=2}^{\infty} (v_i/v_{visc})^j/j! \tag{14}$$

we finally obtain v_i as an inverse function of λ, $v_i(\lambda) = \lambda^{-1}[\lambda(v_i)]$.

Dynamic effects can be expected when the driving force varies abruptly, for instance, when the moving dislocation meets with obstacles; additionally, the moving dislocation should have enough kinetic energy or, equivalently, the drag coefficient B should be small enough so that dislocation motion can be underdamped [3, 8–10]. Then the dislocation after an activation event can reach a dynamic overshooting configuration at the next obstacle so that the dislocation angle of attack becomes larger than the static angle θ. This results in an increase of the dislocation force on the obstacle above the static force F. Such an effect can be taken into account by a dynamic parameter δ, if we include into equation (11) an additional term, $\Gamma(\partial^2 y/\partial x^2)$, and solve it with standard boundary and initial conditions, $y(nl,t) = 0$ and $\partial y(x,0)/\partial t = v_i$. Then the dynamic (time-dependent) solution y_d and static solution y_{st} are

$$y_d(x,t) = e^{-\gamma} \sum_{n=0}^{\infty} (C_n \cos \omega_n t + D_n \sin \omega_n t) \sin k_n x \tag{15a}$$

$$y_{st}(x) = b\sigma x(l-x)/2\Gamma \tag{15b}$$

where $\gamma = B/2m = 1/2\tau_r$, $k_n = (2n+1)\pi/l$, $\omega_n = (c_s^2 k_n^2 - \gamma^2)^{1/2}$, c_s is the speed of shear waves, $C_j = -4b\sigma/\Gamma l k_j^3$, and $D_j = \gamma C_j/\omega_j + 4v_i/l\omega_j k_j$, so that we can define the parameter δ as

$$\delta = 1 + (\partial y_d/\partial x)/(\partial y_{st}/\partial x)|_{x,t} \tag{16}$$

From equations (15a), (15b) and (16) and at the maximum overshooting (at $t = t_{max}$), the parameter δ is now

$$\delta = 1 + e^{-\gamma t_{max}} \sum_{n=0}^{\infty} -\frac{8\cos\omega_n t_{max}}{\pi^2(2n+1)^2} + \left[-\frac{8\gamma}{\pi^2(2n+1)^2} + \frac{8v_i\Gamma}{b\sigma l^2}\right]\frac{\sin\omega_n t_{max}}{\omega_n}. \tag{17}$$

As can be seen, the parameter δ reflects an average

† Landau [14] first introduced a similar function through a fraction of obstacles overcome athermally.

‡ Relativistic effects can be incorporated using a relativistic expression for the effective mass m in equation (11) [16].

dynamic increase of the force F exerted on an obstacle by underdamped dislocation segments of quasi-straight dislocation. Such a parameter was introduced in somewhat simplified and different form in the first inertial models [8–10]. However, its application for dislocation motion was completely different and, as shown later [11], was valid only at stresses close to σ_c. It is seen from equation (17) that δ depends explicitly not only on the applied stress but also on the drag coefficient B through the coefficient γ. Since only a short time is required for the dislocation to cross the activation path y_u–y_s (as specified in Appendix A), the largest first-order term in the series of equation (17) is of main importance. The higher order terms can be neglected since they correspond to longer waves and affect only the specific shape of dislocation line. Such a definition of δ neglects "unzipping" processes, e.g. such as observed in the first computer simulation of dislocation motion through an array of random obstacles at $T = 0$ K [17]. However, the simulation of thermally activated dislocation motion [21] revealed no "unzipping"; instead, the average distance between successive activation sites (which can characterize the "activated unzipping") was found to be in a range between about $4l$ and $30l$, depending on temperature.

Introducing now the critical drag coefficient $B_c = 2\pi\Gamma/lc_s$ to normalize B as $B* = B/B_c$ [12] yields

$$\delta = 1-\frac{8}{\pi^2}e^{-\gamma_{max}}\cos\omega_0 t_{max} + \frac{4}{\pi^2}\left[-2 + \frac{v_i/v_{visc}}{B*^2}\right]\frac{B*}{\sqrt{1-B*^2}}e^{-\gamma_{max}}\sin\omega_0 t_{max} \quad (18)$$

$$t_{max} = \frac{B*}{2\gamma\sqrt{1-B^{*2}}}\left\{\pi + 2\tan^{-1}\frac{B*[2-(v_i/v_{visc})]}{(v_i/v_{visc})\sqrt{1-B^{*2}}}\right\}. \quad (19)$$

As stress increases and/or temperature decreases, $B*$ becomes smaller until at $B^*<1$ the underdamped conditions are reached, $\delta>1$, and breakaways start occurring more often than under the overdamped conditions $\delta<1$. Obviously, the average swept area $\bar{a}$ and the increase δa are not described any more by equations (8) and (9) since they should be converted into dynamic quantities $\bar{a}_d$ and δa_d, together with λ_d. We can obtain them using the scaling relation of equation (5c): a dynamic increase of the force $F*$ by the dynamic factor δ is translated into the respective increase of the stress $\sigma*$ as $\sigma*_d = \delta^{3/2}\sigma*$ in equations (9) and (10). Then the average total dislocation velocity of equation (1) becomes

$$v_{total} = \frac{L^2}{l(1-\delta a_d)\{v_d^{-1}\exp(\Delta G*_{eff}/T*)-\tau_r\ln[1-(v_i/v_{visc})]\}} \quad (20)$$

where l and ΔG^*_{eff} depend only on σ, τ_r only on T, and δa_d, v_i and v_{visc} on both σ and T.

3. EVALUATION OF DRAG COEFFICIENT

3.1. Phonon drag mechanisms

In the previous section, we demonstrated how to derive the dislocation velocity expression taken the dynamic effects into account. Since they depend on the drag coefficient B, we now consider in more detail the temperature dependence $B(T)$. Experimental data are in a good agreement with theoretical predictions but available only for several metals; therefore, we use a recent comprehensive overview given by Alshits [5] to calculate main contributions into $B(T)$. We start with the phonon drag theory, the underlying concept of which is the phonon–dislocation interaction as a main mechanism of energy dissipation leading to a viscous drag on the moving dislocation. Additionally, all the specific drag mechanisms should be considered within the framework of the same consistent formalism. Correspondingly, three main phonon contributions into dislocation drag are distinguished: the flutter mechanism is dominant at low temperatures, the phonon wind mechanism at intermediate temperatures, and phonon–phonon interaction at higher temperatures. Several other possible phonon mechanisms are neglected as insignificant [5].

The flatter contribution B_{fl} appears due to processes of reradiation of phonons by a dislocation oscillating in the thermal field of the lattice. The theory predicts $B_{fl}\propto T^3$ at temperatures much lower than the Debye temperature θ_D. Anharmonic strain field scattering of phonons by the moving dislocation is responsible for the so-called phonon "wind" contribution B_w. At low temperatures, $B_w\propto T^5$ but the dependence changes into linear at higher temperatures. The slow-phonon viscosity mechanism might be important if the dislocation is oriented parallel to the group velocity of phonons from flat regions on the isofrequency surface of the phonon spectrum. The contribution of this mechanism, B_{vs} into the total drag can be comparable with B_w at high temperatures but it depends on specific features of the phonon spectrum of a given material.

The numerical calculations for typical metals show that the combined phonon contribution, B_{ph}, is less than about 0.1 μPa·s at low temperatures of $T\leq$ 10 K and between 30 and 80 μPa·s at room temperature. The contributions of the discussed phonon mechanisms are shown in Fig. 2 at $0<T\leq\theta_D$ calculated [25] for a model material with copper parameters, with a dislocation cutoff radius of $r_0 = 3b$ and Murnaghan's factors for copper elastic constants of the third order according to [5]. The analytical expressions for each contribution into $B(T)$ are also taken from [5].

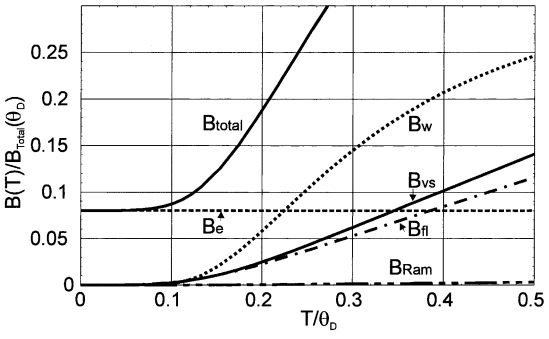

Fig. 2. Relative contributions of main drag mechanisms into the total dislocation drag coefficient B_{total}.

3.2. Effect of the Peierls barrier on dislocation drag

Although our model assumes that the dislocation–obstacle interaction is predominant in the resistance to the dislocation glide, the Peierls barrier τ_p might affect the dislocation drag. Theoretical studies show [5] that the Peierls barrier can be responsible for two types of mechanisms: additional energy dissipation because of oscillation of the strain field of a dislocation during its viscous motion over the barrier and a "dry radiation friction" component. The former results in a new drag contribution B_{Ram}, mainly due to inelastic (Raman) scattering, where B_{Ram} has the same functional form as B_w. Then the contribution can be presented as $B_{Ram} = IB_w$, where I is a temperature independent factor changing linearly with the ratio τ_p/μ and typically between 0.01 and 0.1. The other, radiation mechanism leads to more complex dislocation behavior, which depends on the dislocation velocity, the Peierls stress, the total drag and details of the Peierls barrier. When $\sigma > \tau_p$, the radiation can be included by renormalizing the applied stress σ to $\sigma - \tau_{dP}$, where τ_{dP} is the "dynamic" Peierls stress [5]. Since τ_{dP} is typically less than τ_p, we neglected this effect. A small contribution of B_{Ram} is shown in Fig. 2 for $I = 0.056$ calculated according to the assumed value of τ_p.

3.3. Electron drag mechanisms

Like phonons, conduction electrons contribute to the drag B since a moving dislocation also scatters electrons. Kravchenko [28] and Hollstein [29] were the first who estimated the dislocation electron drag B_e in normal metals. Although they used different models (an electron-transport theory in [28] and perturbation scattering theory in [29]), both obtain a similar temperature-independent formula,

$$B_e = Cbn_e p_F \tag{21}$$

where n_e and p_F are the density and the Fermi momentum of electrons, but with different numerical constants C. Depending on the dislocation type, C is between 0.01 and 0.2 for ordinary metals, so that B_e is roughly between 0.2 and 5 μPa·s. We estimate the electron drag for our Cu-prototype material using a free electron model and find from equation (21) that $B_e \approx 3.0\ \mu$Pa·s. As evident from Fig. 2, B_e becomes comparable with or larger than the phonon drag at $T \leq 0.15\theta_D$. Alshits [30] suggested that, similar to the slow phonons drag mechanism, an additional electron drag could exist in metals with flat sections of the Fermi surface. The contribution is due to the relaxation of electrons whose group velocity is parallel to the dislocation. This might be important in metals with more complicated than spherical Fermi surfaces, such as Mo or W, so that we exclude this contribution from our calculations for this paper.

4. CALCULATION RESULTS AND DISCUSSION

In all calculations, we use a set of parameters corresponding to a prototype f.c.c. metal, which we choose to be close to copper. Since we assume weak obstacles, the total free enthalpy is $G_0 = 0.5$ eV, $\Delta G^*_{eff}(\sigma^*)$ is taken from curve (d) of Fig. 1 and the attempt dislocation frequency ν_d is a commonly used value of $\nu_d = 10^{11}$Hz $\approx 0.01\nu_D$, where ν_D is the Debye frequency [3, 6]. We consider the chosen form of $\Delta G_{eff}(\sigma^*)$ as a convenient model curve and not as the dependence representing specific dislocation–obstacle interaction. If a realistic dislocation–obstacle interaction potential is developed, it can be easily incorporated in equation (20). The determining factors in dislocation velocity calculation are not specific parameters p and q but G_0 and σ_c in equation (6). The other parameters are $b = a/\sqrt{2} = 0.255$ nm, $\theta_D = 343$ K, $\rho = 8.96\times10^3$ kg/m^3, $\mu = 54.6$ GPa, $c_s = 2.47\times10^3$ m/s, $\alpha = 0.564$ and $\alpha_F = 1.082$ [25]. Renormalization can easily adjust the obtained results to materials with other parameters.

The results of calculation of the reduced drag coefficient B^* as a function of the applied stress is shown in Fig. 3 for various reduced temperatures to indicate the range of $B^* \leq 1$ required for the dynamic effect. As can be seen, the effect starts near the critical stress at $T^* \leq 0.014$ but observed over almost the entire low-

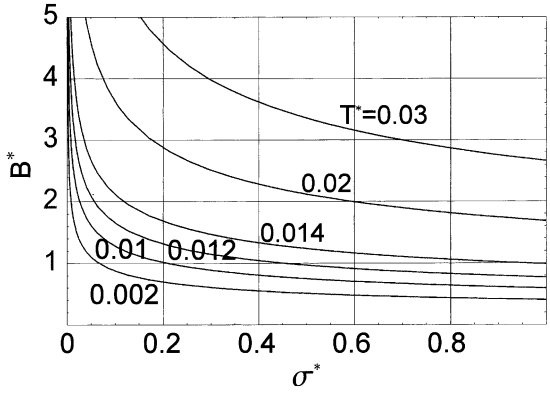

Fig. 3. Dependence of B^* on σ^* at different temperatures T^* for obstacles with $\theta_c = 15.15°$, $L = 1000a$, and $\sigma_c = 2$ MPa.

stress region as temperature reduces to $T* \leq 0.01$. Comparison of Fig. 3 with Fig. 2 (where temperature was normalized by $\theta_D = 343$ K instead of G_0/k in Fig. 3) shows that the dynamic effect begins when the phonon drag demonstrates a considerable decline below $T \approx 60$ K. Since B^* depends linearly on the dislocation segment length (through the critical drag coefficient B_c), the dynamic effect depends not only on temperature and stress but also on the density of obstacles.

The dynamic overshooting requires another condition to occur: the relaxation time τ_r should be comparable to the oscillation period during the underdamped collision process. Our calculations show that τ_r remains rather short, between 100 and 8 ps, as the temperature changes from 10 to 300 K. Hence, dislocation velocity reaches the final viscous velocity very fast in the low-velocity region, so that one can replace the impact velocity by the viscous velocity in majority of calculations, except for cases where the running time is comparable to the relaxation time. Such a simplification is employed in other calculations [31] and seems to be a reasonable approximation in certain ranges of material parameters.

The relative dynamic increase δa_d of the average swept area is shown in Fig. 4 as a function of the applied stress at different temperatures. As temperature decreases, the entire dependence $\delta a_d(\sigma^*)$ moves towards lower stresses indicating that the dislocation travels a longer path between metastable configurations at lower temperatures of $T* \leq 0.014$. At higher temperatures of $T* \geq 0.02$, all the curves are overlapped corresponding to the static equation (9) with no dynamic effect.

A plot summarizing the calculation results of the dependence $v^*(\sigma^*,T^*)$ is shown in Fig. 5, where $v* = v/c_s$ and c_s is the speed of shear waves. The plot explicitly demonstrates the main experimentally observed feature of dislocation motion: two ranges with significantly different temperature and stress dependences. The velocity v^* changes with σ^* nonlinearly at $v* \leq 10^{-4}$ and at almost all σ^*; additionally, v^* considerably increases with temperature, which is typical of the thermal activation region. The stress dependence $v^*(\sigma^*)$ in this region becomes considerably steeper as temperature decreases, which is also consistent with all experimental findings [4]. On the other hand, the dependence becomes linear at higher v^* and, as expected, the temperature dependence $v^*(T^*)$ is also reversed within this region. Such behavior is often identified with drag-dependent processes that can appear only at $\sigma* \geq 1$. However, as seen from Fig. 5, the linear dependence can start much earlier (for instance, from $\sigma* \approx 0.65$ at $T* = 0.01$) revealing the dynamic effect at low temperatures. This is a clear indication of coupling all of the three mechanisms considered in this model. At small stresses, the activation events dominate the process, and the contributions of the drag-dependent running time t_{run} and inertial overshooting are insignificant. As the stress increases, the average swept area becomes larger, so that the contribution of both t_{run} and inertia also increases. Since the latter two processes are the reverse of each other, the dislocation behavior reflects all of three processes at the inter-

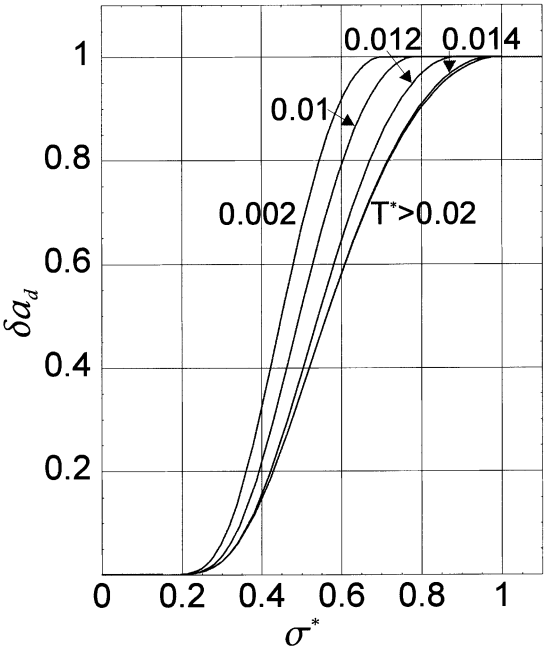

Fig. 4. Effect of temperature on the relative dynamic increase δa_d of the swept area for the model material of Fig. 3.

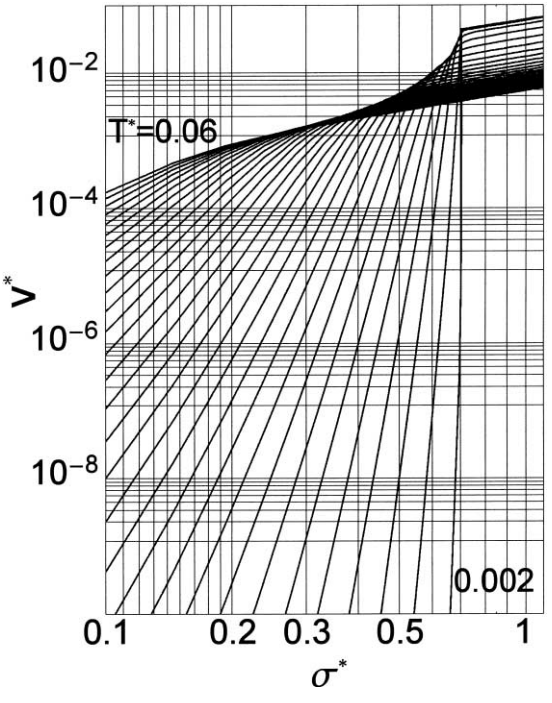

Fig. 5. Dependence of v^* on σ^* at different temperatures T^* (with 0.002-increments) for the model material of Fig. 3.

mediate stress range $\sigma* \leq \sigma_c$ where λ_d and t_{run} are large enough to determine the linear dependence $v^*(\sigma^*)$.

The influence of the obstacle concentration (through the average obstacle spacing L) on the dislocation velocity is shown in Fig. 6 at $T* = 0.02$ for weaker obstacles ($\theta_c = 3.26°$). In these calculations, the applied stress is normalized to obtain $\sigma_c = 2$ MPa at $L = 100a$, and L is changed over one order of magnitude, from $100a$ to $1000a$. Fig. 6 indicates that an increase in the obstacle concentration affects the dependence $v^*(\sigma^*)$ by shifting it to higher stresses, where the obstacle-controlled mechanism is prevalent; at the same time, the velocity in the drag-dependent region remains the same. Similar behavior has been observed experimentally in copper after irradiation and in copper-based alloys.† As can also be seen, the dislocation velocity changes dramatically with the obstacle concentration. For instance, the tenfold increase in L at $\sigma* = 0.1$ causes the velocity to increase by almost ten orders of magnitude.

The obtained features of dislocation motion can be compared with macroscopical plastic deformation by calculating such quantities as the stress required to move a dislocation with a given constant velocity and the velocity sensitivity, $d\sigma*/d(\ln v*)$, at various temperatures. From the Orowan equation and with an assumption of a constant dislocation density, the former is an equivalent of the yield stress σ_y and the latter of the strain rate sensitivity $s = \Delta\sigma/\Delta \ln\dot{\varepsilon}$, where $\dot{\varepsilon}$ is the strain rate. Fig. 7 explicitly demonstrates two interesting features of dislocation behavior at low temperatures mentioned above. The calculations are carried out for $L = 500a$, $\sigma* = 2$ MPa, and weaker obstacles than in Fig. 3 ($\theta_c = 9.53°$). The first feature is the "anomalous flow stress behavior", i.e. a positive temperature dependence of the stress σ^* between $T* \approx 0.005$ and $T* \approx 0.01$, with a peak determined by the velocity v^*. Unlike such an anomaly in intermetallics at high temperatures (e.g. an overview given in Yoo *et al.* [32] on mechanical properties and dislocation velocity measurements in [33]), the dependence is a result of competition between the phonon drag increase with temperature, which requires higher stresses, and an activation rate increase with temperature, which requires lower stresses, to maintain a constant dislocation velocity. In this specific region, the drag-dependent effect is larger and this causes the stress to rise. This kind of anomaly has been found experimentally in copper–aluminum alloys at low temperatures [34].

The second feature, a constant "yield stress" is observed at $T* \leq 0.004$. Such an "athermal" plateau has been observed in many materials, and there were many attempts to attribute it to quantum phenomena (e.g. reviewed in Suzuki [34]). Instead, as Figs 5 and 7 indicate, a simpler explanation is a steep stress dependence of the dislocation velocity at low temperatures that results in such a practically unchanging stress.

Finally, the behavior of the dislocation velocity sensitivity calculated from the velocity dependence $v^*(\sigma^*,T^*)$ is shown in Fig. 8. The sensitivity increases with temperature over almost the entire stress region; additionally, the sensitivity increases almost linearly with the stress at higher T^* but changes only "slightly" at low T^*, which is again attributed to the steep $v^*(\sigma^*)$ dependence in this region.

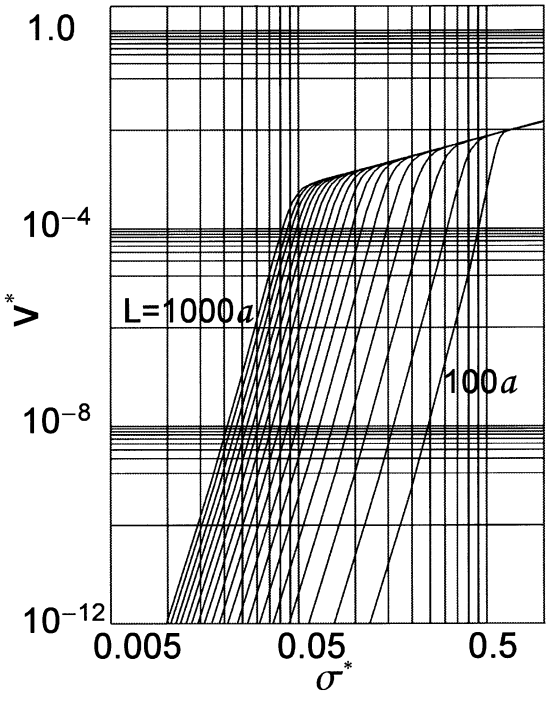

Fig. 6. Dependence of v^* on σ^* at various L (with $100a$-increments), $\theta_c = 3.26°$.

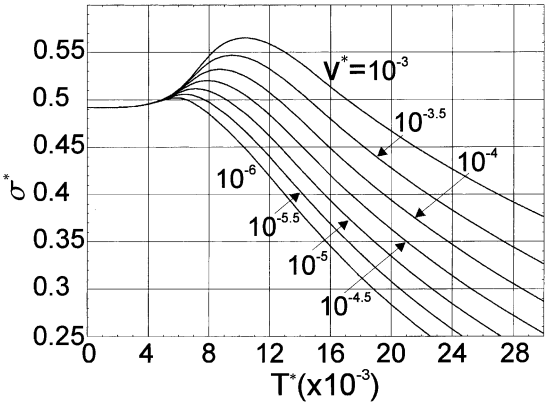

Fig. 7. Effect of temperature T^* on the stress σ^* necessary to move the dislocation with the shown constant velocity v^*, $\Theta_c = 9.53°$.

† A combined v–σ plot of experimental results obtained in pure copper and its alloys is shown in Fig. 6.22 [4].

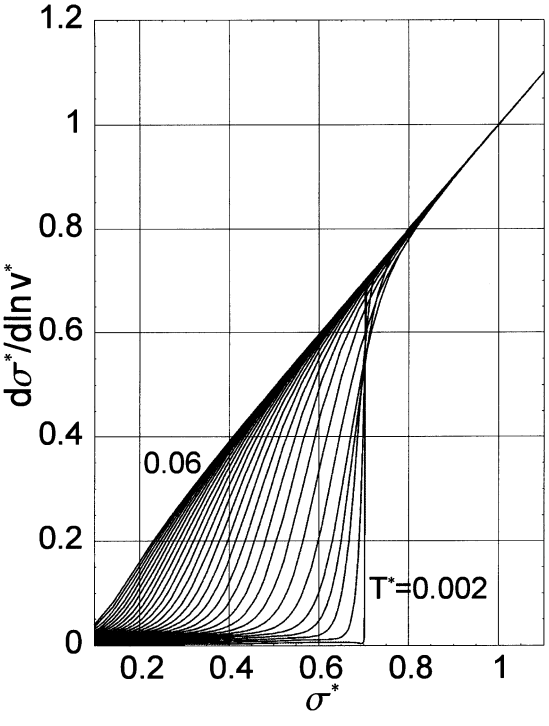

Fig. 8. Dependence of $d\sigma*/d(\ln v*)$ on σ^* at different temperatures T^* (with 0.002-increments) for the model material of Fig. 3.

5. CONCLUDING REMARKS

The results of calculations based on a phenomenological model of dislocation motion applied to a prototype f.c.c. metal are presented in this paper. The model explicitly takes into consideration three stages of dislocation motion through arrays of random discreet obstacles: thermally activated breakaway from obstacles at an equilibrium position, the accelerated drag-dependent run to the next obstacles, and a dynamic transition to the next equilibrium position. The stress dependence of the dislocation velocity at various temperatures and concentrations of obstacles is obtained for the first time with such stages. The calculations show that the third stage can be essential for the dislocation–obstacle collisions when the obstacle concentration is high, even at such temperatures that phonon drag is not frozen out. All of the three stages can make comparable contributions in the intermediate region of $v(\sigma,T)$ between the obstacle-dependent and drag-dependent regions where velocity calculations have not been performed until now. In this region, a competition between thermal activation and inertia produces complicated dislocation velocity dependences on model parameters. The model reveals several new features in dislocation dynamics and demonstrates a good qualitative agreement with experimental data, suggesting that the model is appropriate for the description of dislocation behavior near the yield point. Obviously, the current model should be advanced to include other materials, the anisotropy of the dislocation line tension, different types of dislocations, and various dislocation–obstacle-interactions.

Acknowledgements—One of the authors (M.H.) would like to show appreciation for the support from the Pacific Northwest National Laboratory.

REFERENCES

1. Messerschmidt, U., *Z. Metall.*, 1993, **84**, 391.
2. Kaganov, M. I., Kravchenko, B. Y. and Natsik, V. D., *Soviet Physics-Uspekhi*, 1974, **16**, 878.
3. Kocks, U. F., Argon, A. S. and Ashby, M. F., *Thermodynamics and Kinetics of Slip* (*Progress in Materials Science*, Vol. 19). Pergamon Press, Oxford, 1975.
4. Nadgorny, E., *Dislocation Dynamics and Mechanical Properties of Crystals* (*Progress in Materials Science*, Vol. 31). Pergamon Press, Oxford, 1988.
5. Alshits, V. I., in *Elastic Strain Fields and Dislocation Mobility*, ed. V. L. Indenbom and J. Lothe. Elsevier Science, Amsterdam, 1992, p. 625.
6. Indenbom, V. L. and Chernov, V. M., in *Elastic Strain Fields and Dislocation Mobility*, ed. V. L. Indenbom and J. Lothe. Elsevier Science, Amsterdam, 1992, p. 517.
7. Frost, H. J. and Ashby, M. F., *J. Appl. Phys.*, 1971, **42**, 5273.
8. Suenaga, M. and Galligan, J. M., *Scripta metall.*, 1971, **5**, 829.
9. Granato, A. V., *Phys. Rev. B*, 1971, **4**, 2196.
10. Komada, K. and Yoshiyama, Y., *J. Phys. Soc. Japan*, 1971, **31**, 1056.
11. Estrin, Y. Z., *Soviet J. Low Temp. Phys.*, 1975, **1**, 45.
12. Schwarz, R. B. and Labush, R., *J. Appl. Phys.*, 1978, **49**, 5174.
13. Schwarz, R. B., *Phys. Rev. B*, 1980, **21**, 5617.
14. Landau, A. I., *Physica Status Solidi (a)*, 1980, **61**, 555.
15. Isaac, R. D. and Granato, A. V., *Phys. Rev. B*, 1988, **37**, 9278.
16. Hirth, J. P., Zbib, H. M. and Lothe, J., *J. Model. Simul. Mater. Sci. Engng*, 1998, **6**, 165.
17. Foreman, A. J. E. and Makin, M. J., *Phil. Mag.*, 1966, **14**, 911.
18. Hanson, K. and Morris, J. W., *J. Appl. Phys.*, 1975, **46**, 983.
19. Labusch, R., *J. Appl. Phys.*, 1977, **48**, 4550.
20. Zaitsev, S. I. and Nadgorny, E. M., *Soviet Phys. Solid State*, 1974, **15**, 1777.
21. Zaitsev, S. I. and Nadgorny, E. M., *Nuclear Metall.*, 1976, **20**, 707.
22. Zaitsev, S. I. and Nadgorny, E. M., *Nuclear Metall.*, 1976, **20**, 816.
23. Zaitsev, S. I., Kirsanov, V. V. and Tyupkina, O. G., *Soviet Phys. Solid State*, 1983, **25**, 1247.
24. Friedel, J., *Dislocations*. Pergamon Press, Oxford, 1964.
25. Hiratani, M., Ph.D. thesis, Michigan Technological University, Houghton, 2000.
26. Klahn, D. H., Austin, D., Mukherjee, A. K. and Dom, J. E., in *Advances in Applied Probability, Suppl. 2* 1973, 112.
27. Landau, A. I., *Physica Status Solidi (a)*, 1981, **65**, 119.
28. Kravchenko, V. Y., *Soviet Phys. Solid State*, 1966, **8**, 740.
29. Hollstein, T., *Phys. Rev.*, 1966, **151**, 187.
30. Alshits, V. I., *Soviet Phys. JETP*, 1975, **40**, 1099.
31. Rhee, M., Zbib, H. M., Hirth, J. P., Huang, H. and de la Rubia, T., *J. Model. Simul. Mater. Sci. Engng*, 1998, **6**, 467.
32. Yoo, M. H., Sass, S. L., Fu, C. L., Mills, M. J., Dimiduk, D. M. and George, E. P., *Acta metall. mater.*, 1993, **41**, 987.
33. Nadgorny, E. M. and Iunin, Y. L., *Mater. Res. Soc. Symp. Proc.*, 1995, **364**, 707.
34. Suzuki, T., in *Micromechanics of Advanced Materials*, ed.

S. N. G. Chu, P. K. Liaw, R. J. Arsenault and K. Sadananda. MMMS, 1995, p. 73.
35. Cottrell, A. H., *Dislocations and Plastic Flow in Crystals*. Clarendon Press, Oxford, 1953.

APPENDIX A

A.1. Activation free enthalpy for dislocation thermally activated motion

As an example, consider the simplest case of an edge dislocation and an obstacle representing a point source of dilatation [6]. The straight dislocation is oriented along the *y*-direction and glides on the *xy*-plane under an applied stress, while the immobile obstacle is at point $(0,0,z_0)$. In the linear elasticity approximation for isotropic media, the dislocation–obstacle interaction energy is

$$U_{\mathrm{int}}(y,z) = \frac{\mu b_{\mathrm{e}}(1+\nu)z}{3\pi(1-\nu)r^2}\delta V \tag{A1}$$

or, after normalization,

$$U*_{\mathrm{int}}(y) = U_{\mathrm{int}}/U_0 = [1 + (y/z_0)^2]^{-1} \tag{A2}$$

where $r = \sqrt{y^2 + z_0^2}$ is the shortest distance between the dislocation and the obstacle, δV the dilatation volume, ν Poisson's ratio, and the maximum interaction energy $U_0 \equiv U_{\mathrm{int}}(y = 0)$.

Then the obstacle force profile [35] that is the dependence $F(y)$ of the force exerted by the obstacle on the dislocation line is

$$F = -\delta U_{\mathrm{int}}/\delta y = 2z_0U_0yz/(y^2 + z^2)^2 \tag{A3}$$

which has an extreme value at $y = \pm z_0/\sqrt{3}$, equals zero at the origin, and in the reduced form becomes

$$F*(y*) = 16y*/3\sqrt{3}(1 + y*^2)^2 \tag{A4}$$

where $y* = y/z_0$ and $F* = F/F_{\max}$ (The maximum force $F_{\max}$ corresponds to the critical force F_{c}.) When the dislocation glides, it stops at its first stable equilibrium position of $y = y_{\mathrm{s}}$. At this position, the force F balances the opposing force F' applied by the dislocation on the obstacle, and thermal activation is required to move the dislocation forward through an activation-energy barrier. The next equilibrium position at $y = y_{\mathrm{u}}$ is unstable, so that the dislocation can continue to move leaving the obstacle behind.

The activation-energy (or rather free enthalpy) barrier ΔG depends on the force exerted by the dislocation on the obstacle. At zero force, ΔG is at its maximum corresponding to the total free enthalpy, $\Delta G(0) = G_0$; ΔG is zero when the force reaches $F_{\max}$. Using a conventional procedure [3, 6], ΔG can be derived as a function of the obstacle force F, which in the case under consideration takes a form of

$$\begin{aligned}\Delta G &= \int_{y_{\mathrm{s}}}^{y_{\mathrm{u}}} F(y*)\,\mathrm{d}y - (y*_{\mathrm{u}} - y*_{\mathrm{s}})F*_0 \\ &= (8\sqrt{3}/9)[(y*_{\mathrm{u}}^2 + 1)^{-1} - (y*_{\mathrm{s}}^2 + 1)^{-1}] \\ &\quad -(y*_{\mathrm{u}} - y*_{\mathrm{s}})F*_0\end{aligned} \tag{A5}$$

where y_{s} and y_{u} are the equilibrium stable and unstable positions of the dislocation, respectively, and $F*_0 = F*(y*_{\mathrm{s}}) = F*(y*_{\mathrm{u}})$. Equations (A4) and (A5) combine to obtain y_{s} and y_{u} from the equation

$$y*^4 + 2y*^2 - (16/3\sqrt{3}F*_0)y* + 1 = 0. \tag{A6}$$

Solving equation (A6) with routine procedures for biquadratic and tri-polynomial equations yields

$$y*_{\mathrm{u}} = \mathrm{sgn}(F*_0)(-\sqrt{t_1 - \tfrac{1}{3}} + \sqrt{t_2 - \tfrac{1}{3}} + \sqrt{t_3 - \tfrac{1}{3}}) \tag{A7a}$$

$$y*_{\mathrm{s}} = \mathrm{sgn}(F*_0)(-\sqrt{t_1 - \tfrac{1}{3}} - \sqrt{t_2 - \tfrac{1}{3}} - \sqrt{t_3 - \tfrac{1}{3}}) \tag{A7b}$$

where $t_1 = (s + s^{-1})/3$, $t_2, t_3 = -t_1/2 \pm (s - s^{-1})(i/2\sqrt{3})$, $s = -3b/2 + \sqrt{9b^2/4 - 1/81}$, and the constant $b = (2/27) - (4/27F*_0^2)$. From equations (A5), (A7a) and (A7b) the dependence $\Delta G*(F*)$ can now be obtained to satisfy equation (2) (Fig. 1, curve d), with the fitting parameters $p = 0.63$ and $q = 1.63$.